

# X-ray illumination of the ejecta of Supernova 1987A

J. Larsson<sup>1</sup>, C. Fransson<sup>1</sup>, G. Östlin<sup>1</sup>, P. Gröningsson<sup>1</sup>, A. Jerkstrand<sup>1</sup>, C. Kozma<sup>1</sup>, J. Sollerman<sup>1</sup>, P. Challis<sup>2</sup>, R. P. Kirshner<sup>2</sup>, R. A. Chevalier<sup>3</sup>, K. Heng<sup>4</sup>, R. McCray<sup>5</sup>, N. B. Suntzeff<sup>6</sup>, P. Bouchet<sup>7</sup>, A. Crotts<sup>8</sup>, J. Danziger<sup>9</sup>, E. Dwek<sup>10</sup>, K. France<sup>11</sup>, P. M. Garnavich<sup>12</sup>, S. S. Lawrence<sup>13</sup>, B. Leibundgut<sup>14</sup>, P. Lundqvist<sup>1</sup>, N. Panagia<sup>15,16,17</sup>, C. S. J. Pun<sup>18</sup>, N. Smith<sup>19</sup>, G. Sonneborn<sup>10</sup>, L. Wang<sup>20</sup>, J. C. Wheeler<sup>21</sup>

<sup>1</sup>*Department of Astronomy, The Oskar Klein Centre, Stockholm University, 106 91 Stockholm, Sweden.*

<sup>2</sup>*Harvard-Smithsonian Center for Astrophysics, 60 Garden Street, MS-19, Cambridge, MA 02138, USA.*

<sup>3</sup>*Department of Astronomy, University of Virginia, Charlottesville, VA 22903, USA*

<sup>4</sup>*Eidgenössische Technische Hochschule Zürich, Institute for Astronomy, Wolfgang-Pauli-Strasse 27, CH-8093, Zürich, Switzerland.*

<sup>5</sup>*JILA, University of Colorado, Boulder, CO 803090-0440, USA.*

<sup>6</sup>*George P. and Cynthia Woods Mitchell Institute for Fundamental Physics and Astronomy, Texas A&M University, Department of Physics and Astronomy, College Station, TX 77843, USA.*

<sup>7</sup>*DSM/IRFU/Service d'Astrophysique Commissariat à l'Énergie Atomique et aux Énergies Alternatives, Saclay, Orme des Merisiers, FR 91191 Gif-sur-Yvette, France.*

<sup>8</sup>*Department of Astronomy, Mail Code 5240, Columbia University, 550 West 120th Street, New York, NY 10027, USA.*

<sup>9</sup>*Osservatorio Astronomico di Trieste, Via Tiepolo 11, Trieste, 34131, Italy.*

<sup>10</sup>*NASA Goddard Space Flight Center, Code 665, Greenbelt, MD 20771, USA.*

<sup>11</sup>*Center for Astrophysics and Space Astronomy, University of Colorado, Boulder, CO 80309, USA.*

<sup>12</sup>*225 Nieuwland Science, University of Notre Dame, Notre Dame, IN 46556-5670, USA.*

<sup>13</sup>*Department of Physics and Astronomy, Hofstra University, Hempstead, NY 11549, USA.*

<sup>14</sup>*ESO, Karl-Schwarzschild-Strasse 2, 85748 Garching, Germany.*

<sup>15</sup>*Space Telescope Science Institute, 3700 San Martin Drive, Baltimore, MD 21218, USA.*

<sup>16</sup>*INAF-CT, Osservatorio Astrofisico di Catania, Via S. Soa 78, I-95123 Catania, Italy.*

<sup>17</sup>*Supernova Limited, OYV #131, Northsound Road, Virgin Gorda, British Virgin Islands.*

<sup>18</sup>*Department of Physics, University of Hong Kong, Pok Fu Lam Road, Hong Kong, China.*

<sup>19</sup>*Steward Observatory, University of Arizona, 933 North Cherry Avenue, Tucson, AZ 85721, USA.*

<sup>20</sup>*Department of Physics and Astronomy, Texas A&M University, College Station, TX 77843-4242, USA.*

<sup>21</sup>*Department of Astronomy, University of Texas, Austin, TX 78712-0259, USA.*

**When a massive star explodes as a supernova, substantial amounts of radioactive elements—primarily  $^{56}\text{Ni}$ ,  $^{57}\text{Ni}$  and  $^{44}\text{Ti}$ —are produced<sup>1</sup>. After the initial flash of light from shock heating, the fading light emitted by the supernova is due to the decay of these elements<sup>2</sup>. However, after decades, the energy for a supernova remnant comes from the shock interaction between the ejecta and the surrounding medium<sup>3</sup>. The transition to this phase has hitherto not been**

**observed: supernovae occur too infrequently in the Milky Way to provide a young example, and extragalactic supernovae are generally too faint and too small. Here we report observations that show this transition in the supernova SN 1987A in the Large Magellanic Cloud. From 1994 to 2001 the ejecta faded owing to radioactive decay of  $^{44}\text{Ti}$  as predicted. Then the flux started to increase, more than doubling by the end of 2009. We show that this increase is the result of heat deposited by X-rays produced as the ejecta interacts with the surrounding material. In time, the X-rays will penetrate farther into the ejecta, enabling us to analyse the structure and chemistry of the vanished star.**

Due to the proximity of SN 1987A (located only 160,000 light years away), we can study the evolution of the supernova (SN) in great detail. The central ejecta are surrounded by a ring of circumstellar material (Fig. 1) that was shed from the star 20,000 years before the explosion in 1987<sup>4</sup>. Since the explosion, the ejecta have been expanding, and now the outer parts of the ejecta are colliding with the ring, causing it to brighten at all wavelengths<sup>5-8</sup>. The dense, central part of the ejecta contains most of the mass from the disrupted star and acts as a calorimeter for the energy input to the SN. We have determined the energy input by tracking the energy output with the Hubble Space Telescope (HST).

Because the ejecta are roughly elliptical in projection on the sky we use an elliptical aperture to measure the brightness. To monitor a constant mass of expanding material, we allowed the measuring aperture to expand linearly with time. The axes of the aperture were therefore three times larger in 2009 than in 1994 (Fig. 1). Using this aperture, we determined the R-and and B-

band light curves of the ejecta, as shown in Fig. 2 (see Supplementary Table 1 and Supplementary Information, section 1 for further details of the observations and light curves). Our measurements show that the flux from the ejecta decays during the first  $\sim 5,000$  days after the explosion, as expected from radioactive input, but then starts to increase, reaching a level that is 2-3 times higher around day 8,000 (end of 2009). A new energy source must be present in addition to radioactive decay. Below, we consider a model for the declining phase and then discuss the new energy source that is responsible for the observed increase in flux.

The energy input to the declining phase of the light curve after  $\sim 1,500$  days is expected to come from positrons produced in the decay of  $^{44}\text{Ti}^{2,9,10}$ . To test this we use a model<sup>2</sup> with abundances taken from the 14E1 explosion model<sup>11</sup> and a  $^{44}\text{Ti}$  mass of  $1.4 \times 10^{-4} M_{\odot}$ <sup>12</sup> (Supplementary Information, section 3). The model is shown in Fig. 3 together with the observed broadband luminosities. The good agreement with the observations up to day 5,000 confirms that the  $^{44}\text{Ti}$  positrons provide the energy input up to this point. However, after day 5,000 the model clearly fails to describe the light curve; radioactive decay cannot explain the increase in flux that we observe.

One possible origin for the flux increase is the reverse shock that results from the interaction between the ejecta and the H II region inside the ring<sup>13-16</sup>. The reverse shock produces strong  $\text{Ly}\alpha$  and  $\text{H}\alpha$  emission, which increased by a factor of  $\sim 1.7$  between 2004 and 2010<sup>16</sup>. Although most of this emission originates close to the ring, there is also a component of projected high-velocity  $\text{H}\alpha$ -emission that can be traced to the central parts of the ejecta<sup>16</sup> and which would therefore

contribute to the flux we measure. To determine the contribution of the reverse shock to our light curves we have examined HST STIS spectra from 2004 and 2010 (Supplementary Information, section 2 and Supplementary Fig. 5). The reverse shock can be isolated in the spectra because of its boxy line profile, allowing us to place a limit on its contribution at  $\lesssim 20\%$ . Furthermore, this changes only marginally between 2004 and 2010, as the expanding measuring aperture remains well inside the area where most of the shock emission is seen. Importantly, an increase in flux is also seen in the [Ca II] doublet lines at rest wavelengths 7,292 Å and 7,324 Å between 2000 – 2010 (determined from UVES observations at the ESO/VLT, Fig. 2). These lines have speeds of  $\lesssim 5,000 \text{ km s}^{-1}$ , implying that they originate in the inner ejecta (the projected ejecta speed near the edge of the ring is  $\gtrsim 7,000 \text{ km s}^{-1}$  at the present time). We conclude that the increase in flux occurs primarily in the inner ejecta and cannot be explained by emission from the shock region.

We believe that the strong X-ray flux produced in the ring collision is the dominant source of energy input to the ejecta. The X-ray flux from the ring increased by a factor  $\sim 3$  in the 0.5 – 10 keV band between day 6,000 and day 8,000<sup>6</sup>, similar to what we find for the optical emission from the ejecta. To investigate this, we calculated the fraction of X-rays absorbed by the ejecta from a point source located at the ring, using the partially mixed 14E1 explosion model<sup>17</sup>. As shown in Supplementary Fig. 6, most of the observed X-ray flux is absorbed in the core region of the ejecta (corresponding to speeds less than  $5,000 \text{ km s}^{-1}$ ), where most of the heavy elements reside. At an energy of  $\sim 0.35 \text{ keV}$ , which corresponds to the temperature of the dominant component in the X-ray spectrum<sup>18</sup>, the fraction of flux absorbed by the ejecta at  $t_{\text{yr}}$  years can be approximated by  $1.6 \times 10^{-3} t_{\text{yr}}^{1.67}$  (the increase with time is mainly due to the increasing solid angle of the expanding

ejecta, assumed to be spherical, as seen from the ring). This gives a present-day absorbed X-ray luminosity of  $\sim 5.0 \times 10^{35} \text{erg s}^{-1}$ . In this calculation we have neglected the weaker, hard component that contributes to the X-ray spectrum<sup>18</sup>. We note that this does not significantly affect the estimate of the absorbed flux, although the hard X-rays may be important due to their larger penetrating power.

To model the ejecta light curve produced by input from the X-rays we scaled the observed X-ray flux<sup>6</sup> by the fraction absorbed at 0.35 keV, multiplied the resulting flux with a constant (corresponding to the conversion efficiency from X-rays to optical) and added this to the radioactive energy input. Fig. 3 shows the scaled X-ray flux together with the observed light curves. This model follows the general trend of the observed fluxes in both bands, although we note that a more accurate model would need to take into account the detailed shape of the X-ray spectrum and the reprocessing of the X-rays into optical emission. The required conversion efficiency from X-rays to optical emission in our model is 5.0% in the R-band and 3.1% in the B-band.

The conversion of X-rays to optical/IR emission is similar to that of the  $^{44}\text{Ti}$  positrons. Both involve degradation of non-thermal electrons to heating, ionization and excitation. For a typical ionization fraction of  $10^{-3} - 10^{-2}$ , the expected efficiency of conversion from X-rays to  $\text{H}\alpha$  (the dominant line in the R-band) is  $\sim 5\%$  (Supplementary Information, section 3). This conversion factor is consistent with the scaling factor we used to model the light curve. Similar arguments apply to the B-band. Furthermore, the density in the core is high enough for the time-scale of recombination to be shorter than the expansion time-scale, ensuring a balance between the energy

input and output.

Other possible explanations for the increase in flux include input from a central pulsar<sup>19</sup>, a transition from optically thick to optically thin dust and positron leakage from the Fe-rich regions. We find that input from a pulsar is unlikely for several reasons. In particular, it would be a strange coincidence for the emission from the pulsar to mimic the increasing X-ray flux from the ring interaction. Also, we expect the energy input from a pulsar to be concentrated toward the low-velocity material at the centre of the ejecta, but observations of the  $H\alpha$  and [Ca II] lines show that the increase occurs for speeds up to  $\sim 5,000 \text{ km s}^{-1}$ . We also note that constraints on a point source at the centre of SN 1987A have already been obtained using HST data taken near the minimum of the ejecta light curve<sup>20</sup>. A change in the properties of the dust or a transition in the positron deposition process are also unable to quantitatively explain the observed increase in flux (Supplementary Information, section 4).

We conclude that SN 1987A has made a transition from a radioactively dominated phase to a phase dominated by the X-ray input from the ring collision. This conclusion has interesting implications for the observed morphology. In particular, most of the X-rays are likely to be absorbed at the boundary of the ejecta core, where the density increases rapidly. This may lead to the light from the ejecta being emitted in a ring that is concentrated to the plane of the circumstellar ring. The 'hole' in the ejecta (Fig. 1), which has become more pronounced since  $\sim 2001$ , may in fact be a result of this, rather than reflecting the true density distribution or dust obscuration. The asymmetric morphology seen at speeds of  $\lesssim 3,000 \text{ km s}^{-1}$  in the near-IR [Si I] and [Fe II] lines<sup>21</sup>

is, however, likely to be intrinsic to the metal core. By studying future changes in the morphology of the ejecta, we will be able to understand the origin of this asymmetry

In the future the density of the ejecta will decrease and the fraction of X-rays absorbed will grow (Supplementary Fig. 7). As a result the ionization will increase and a smaller fraction of the X-ray flux will produce line excitation. A larger fraction will go into heating, leading to an increase in the mid-IR flux and a flattening of the optical light curves. In time, the X-rays will also penetrate deeper layers of the ejecta, thereby allowing us to probe the chemical structure of the innermost ejecta. This will be a novel form of X-ray tomography.



## References

- [1] Woosley, S. E., Heger, A. & Weaver, T. A. The evolution and explosion of massive stars. *Reviews of Modern Physics* **74**, 1015–1071 (2002).
- [2] Fransson, C. & Kozma, C. Radioactivities and nucleosynthesis in SN 1987A. *New Astronomy Review* **46**, 487–492 (2002).
- [3] McKee, C. F. in *Young Supernova Remnants* (eds S. S. Holt & U. Hwang) vol. 565 of *American Institute of Physics Conference Series*, 17–28 (2001).
- [4] Morris, T. & Podsiadlowski, P. The Triple-Ring Nebula Around SN 1987A: Fingerprint of a Binary Merger. *Science* **315**, 1103–1105 (2007).
- [5] Gröningsson, P. *et al.* Time evolution of the line emission from the inner circumstellar ring of SN 1987A and its hot spots. *Astron. Astrophys.* **492**, 481–491 (2008).
- [6] Racusin, J. L. *et al.* X-ray Evolution of SNR 1987A: The Radial Expansion. *Astrophys. J.* **703**, 1752–1759 (2009).
- [7] Zanardo, G. *et al.* Multifrequency Radio Measurements of Supernova 1987A Over 22 Years. *Astrophys. J.* **710**, 1515–1529 (2010).
- [8] Dwek, E. *et al.* Five Years of Mid-infrared Evolution of the Remnant of SN 1987A: The Encounter Between the Blast Wave and the Dusty Equatorial Ring. *Astrophys. J.* **722**, 425–434 (2010).

- [9] Timmes, F. X., Woosley, S. E., Hartmann, D. H. & Hoffman, R. D. The Production of  $^{44}\text{Ti}$  and  $^{60}\text{Co}$  in Supernovae. *Astrophys. J.* **464**, 332–341 (1996).
- [10] Diehl, R. & Timmes, F. X. Gamma-Ray Line Emission from Radioactive Isotopes in Stars and Galaxies. *PASP* **110**, 637–659 (1998).
- [11] Shigeyama, T. & Nomoto, K. Theoretical light curve of SN 1987A and mixing of hydrogen and nickel in the ejecta. *Astrophys. J.* **360**, 242–256 (1990).
- [12] Jerkstrand, A., Fransson, C. & Kozma, C. The  $^{44}\text{Ti}$ -powered spectrum of SN 1987A. *Astron. Astrophys.* (in press); preprint at <http://arxiv.org/abs/1103.3653> (2011).
- [13] Michael, E. *et al.* Hubble Space Telescope Observations of High-Velocity  $\text{Ly}\alpha$  and  $\text{H}\alpha$  Emission from Supernova Remnant 1987A: The Structure and Development of the Reverse Shock. *Astrophys. J.* **593**, 809–830 (2003).
- [14] Smith, N. *et al.* The Reverse Shock of SNR 1987A at 18 Years after Outburst. *Astrophys. J.* **635**, L41–L44 (2005).
- [15] Heng, K. *et al.* Evolution of the Reverse Shock Emission from SNR 1987A. *Astrophys. J.* **644**, 959–970 (2006).
- [16] France, K. *et al.* Observing Supernova 1987A with the Refurbished Hubble Space Telescope. *Science* **329**, 1624–1627 (2010).

- [17] Blinnikov, S., Lundqvist, P., Bartunov, O., Nomoto, K. & Iwamoto, K. Radiation Hydrodynamics of SN 1987A. I. Global Analysis of the Light Curve for the First 4 Months. *Astrophys. J.* **532**, 1132–1149 (2000).
- [18] Zhekov, S. A., Park, S., McCray, R., Racusin, J. L. & Burrows, D. N. Evolution of the Chandra CCD spectra of SNR 1987A: probing the reflected-shock picture. *Mon. Not. R. Astron. Soc.* **721**, 518–529 (2010).
- [19] Woosley, S. E., Hartmann, D. & Pinto, P. A. Hard emission at late times from SN 1987A. *Astrophys. J.* **346**, 395–404 (1989).
- [20] Graves, G. J. M. *et al.* Limits from the Hubble Space Telescope on a Point Source in SN 1987A. *Astrophys. J.* **629**, 944–959 (2005).
- [21] Kjær, K., Leibundgut, B., Fransson, C., Jerkstrand, A. & Spyromilio, J. The 3-D structure of SN 1987A's inner ejecta. *Astron. Astrophys.* **517**, A51–A60 (2010).
- [22] Chugai, N. N., Chevalier, R. A., Kirshner, R. P. & Challis, P. M. Hubble Space Telescope Spectrum of SN 1987A at an Age of 8 Years: Radioactive Luminescence of Cool Gas. *Astrophys. J.* **483**, 925–940 (1997).
- [23] Lucy, L. B., Danziger, I. J., Gouiffes, C. & Bouchet, P. Dust Condensation in the Ejecta of Supernova 1987A - Part Two. In S. E. Woosley (ed.) *Supernovae*, 82–94 (1991).
- [24] Wooden, D. H. *et al.* Airborne spectrophotometry of SN 1987A from 1.7 to 12.6 microns - Time history of the dust continuum and line emission. *Astrophys. J. Supp.* **88**, 477–507 (1993).

## **Supplementary Information**

Supplementary information accompanies this paper.

## **Acknowledgments**

This work was supported by the Swedish Research Council and the Swedish National Space Board. Support for the HST observing program was provided by NASA through a grant from the Space Telescope Science Institute, which is operated by the Association of Universities for Research in Astronomy, Inc.

## **Author contribution**

J.L. carried out the data reduction and analysis together with G.Ö., P.G., B. L., J.S. and P.C.; C.F. performed the theoretical modelling together with A.J. and C.K.; J.L. and C.F. wrote the paper. R.P.K. is PI for the HST/SAINTS collaboration. All authors discussed the results and commented on the manuscript.

## **Author information**

Reprints and permissions information is available at [www.nature.com/reprints](http://www.nature.com/reprints). The authors declare no competing financial interests. Readers are welcome to comment on the online version of this article at [www.nature.com/nature](http://www.nature.com/nature). Correspondence and requests for materials should be directed to J.L. ([josefin.larsson@astro.su.se](mailto:josefin.larsson@astro.su.se)) or C.F. ([claes@astro.su.se](mailto:claes@astro.su.se)).

## Figures

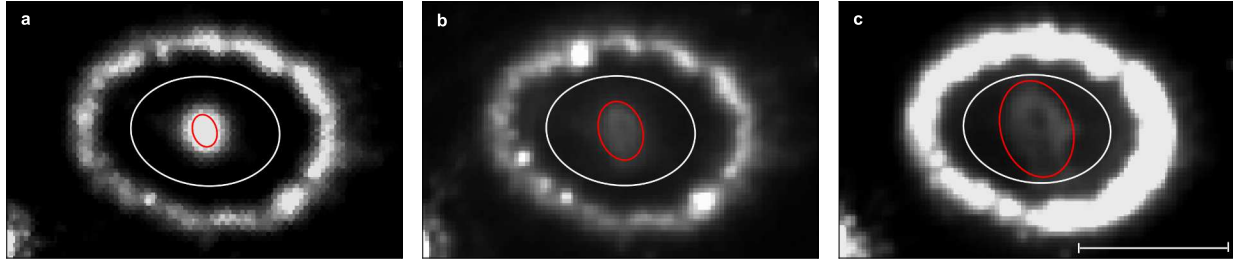


Figure 1: A selection of HST R-band images. The observing dates are 1994-09-24 (**a**), 2000-11-13 (**b**) and 2009-04-29 (**c**), which correspond to 2,770, 5,012 and 8,101 days after the explosion, respectively. The scale bar in **c** represents  $1''$ . The circumstellar ring is inclined at an angle of  $45^\circ$  with respect to the line of sight and is approximately 1.3 light years across. The red (inner) ellipse shows the expanding aperture used for the light curve in Fig. 2. By using an initial semi-major axis of  $0.11''$  for the observation in 1994 we always follow the bright, central part of the ejecta without being significantly affected by emission from the circumstellar ring. The white (outer) ellipse shows the fixed aperture used for one of the light curves in Supplementary Fig. 2. The R-band emission from the ejecta is dominated by  $H\alpha$  emission with a small contribution from [Ca I-II] lines, whereas the B-band (Supplementary Fig. 1) is dominated by H I and Fe I-II lines<sup>12,22</sup>. Only the densest, central parts of the ejecta are visible due to the low surface brightness of the outer parts. In reality, the ejecta extend to the ring, as is evident from the strong interaction with the ring.

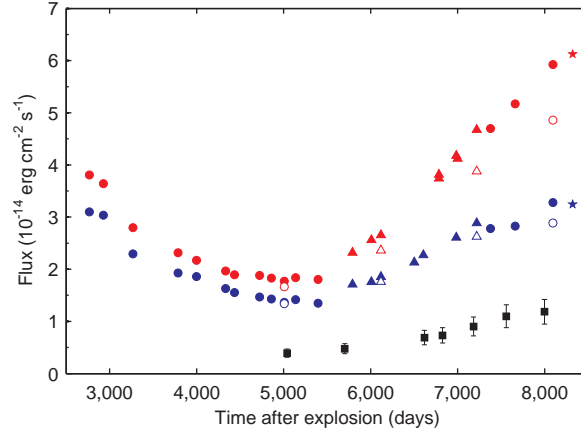


Figure 2: Light curves of the ejecta in different wavebands. Data points from WFPC2, ACS and WFC3 are shown as dots, triangles and stars, respectively. Red and blue symbols correspond to the R- and B-bands. A correction factor has been applied to the ACS and WFC3 fluxes in order to account for the differences between these instruments and WFPC2. To quantify the contamination from the brightening circumstellar ring we created detailed models of the ring for a number of different epochs (Supplementary Information, section 1, and Supplementary Figs. 3 and 4). The open symbols show the ejecta fluxes after the contribution from the ring has been removed. Although the contamination from the ring increases with time it never exceeds  $\sim 20\%$  of the flux from the ejecta. The statistical errors on the HST fluxes are smaller than the data points and systematic errors are discussed in the Supplementary Information, section 1. The black squares show the flux of the [Ca II]  $\lambda\lambda 7291.5, 7323.9$  lines from VLT/UVES (error bars, s.d.). These lines are free from contamination from the circumstellar ring and the reverse shock. We note the decreasing flux during the first  $\sim 5,000$  days and the increase thereafter, indicating an extra source of energy. A further indication that the energy source has changed is that the colour, determined from the flux ratio between the B- and R-bands, changes from a level of  $\sim 0.8$  up to day 5,000 to a value close to  $\sim 0.6$  on day 8,000.

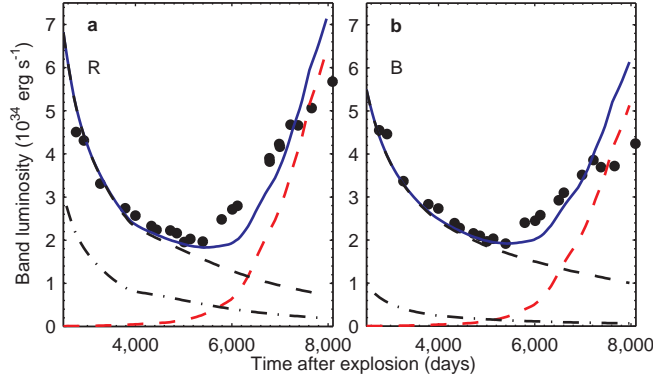


Figure 3: Evolution of the luminosity from the ejecta in the R- and B-bands. The dashed black lines show a model with only radioactive input, mainly from  $^{44}\text{Ti}$ . The  $^{44}\text{Ti}$  mass used for the model is  $1.4 \times 10^{-4} M_{\odot}$ <sup>12</sup>, as determined from a detailed model that takes into account the effects of scattering and fluorescence of the UV flux, as well as a correction for internal dust (here taken to have a 50% covering factor of the core inside  $2000 \text{ km s}^{-1}$ )<sup>23,24</sup>. The lower dot-dashed lines show the light curves with no  $^{44}\text{Ti}$ , illustrating the necessity to include this isotope. The red dashed lines show a model based on a constant fraction of the observed X-ray flux<sup>6</sup>, corrected for the fraction of flux absorbed by the ejecta (Supplementary Fig. 7). The blue solid line shows the sum of both models. The R- and B-bands contain 5% and 3% of the total bolometric flux, respectively, and we expect these fractions to remain roughly constant with time. This is because the relative amount of energy resulting in heating, ionization and excitation will remain nearly constant as long as the ionization by the X-rays is  $\lesssim 10^{-2}$ . It is clear from this figure that there is a transition at  $\sim 5,000$  days from a radioactivity dominated phase to a phase dominated by the X-ray input from the collision with the ring.



# Supplementary information

## 1 Photometry

Our analysis includes all HST imaging observations performed between 1994 and 2009 in the red (WFPC2/F675W, ACS/F625W and WFC3/F675W) and blue (WFPC2/F439W, ACS/F435W and WFC3/F438W) broad-band filters (the two groups of filters will be referred to as the R- and B-bands from here on). The images were drizzled to combine dithered exposures and to remove cosmic rays. Details of the observations are given in Supplementary Table 1 and a selection of images are shown in Supplementary Fig. 1. The images show the expansion of the asymmetric ejecta and the brightening hot spots in the circumstellar ring.

We measured the brightness of the ejecta as a function of time using the IRAF/STSDAS task ELLIPSE, using different elliptical and circular apertures described below. The measurements give mean flux densities, which we convert into total fluxes by multiplying with the rectangular bandwidth of the different filters. When converting to total fluxes we also correct for the fact that there are some differences between the filters used for the three instruments. To determine the corrections we used the HST FOS spectrum from 1997<sup>22</sup> (this covers the entire spectral range probed by all the filters) and used the SYNPHOT package to calculate flux densities in the different filters. After converting to total fluxes we obtain the following flux ratios:  $(\text{ACS/F625W}) / (\text{WFPC2/F675W}) = 1.08$ ,  $(\text{WFC3/F625W}) / (\text{WFPC2/F675W}) = 1.16$ ,

$(\text{ACS}/\text{F435W}) / (\text{WFPC2}/\text{F439W}) = 1.27$  and  $(\text{WFC3}/\text{F438W}) / (\text{WFPC2}/\text{F439W}) = 1.06$ . In all the light curves that we show we have corrected the ACS and WFC3 fluxes in accordance with this. A small offset still remains (see e.g. Fig. 2), which may be due to charge transfer efficiency losses in WFPC2 (see discussion below). Changes in the spectral energy distribution (SED) would also have some effect on the conversion factors, although we note that observations<sup>22,25</sup> suggest that the SED does not vary significantly with time.

For each of the observations we also determined the sky brightness using the IRAF/FITSKY routine. Specifically, we determined the centroid sky value in five empty regions located around SN 1987A and then used the average of these measurements to subtract the sky background from the light curve. The background is typically only a few per cent of the intrinsic ejecta brightness. We also considered the possibility of contamination from the two bright stars that are located to the north-east and south-west of SN 1987A. These stars have strong diffraction spikes from the secondary-mirror spiders, which may pass through the ejecta depending on the HST roll angle. We inspected all the images and found that there is only one observation (2006-04-15) where there is a strong spike passing through our apertures. We estimated the contribution from this spike by measuring the brightness of the other spikes from the same star, and corrected the light curves accordingly. Another source of contamination is one of the narrow outer rings of SN 1987A, which is partly projected on top of the ejecta. However, the small, decreasing flux<sup>26</sup> of this component is negligible compared to the emission from the ejecta.

The shape of the ejecta is roughly elliptical so as a first step we used an elliptical aperture

to measure the evolution of the flux. The shape of the ellipse was determined by fitting elliptical isophotes to the ejecta region in the observation from 2000-11-13. This epoch was chosen because it is long enough after the explosion that the ejecta shape is clearly discernible, while still early enough for the edge of the inner ejecta to be clearly separated from the circumstellar ring. The fits were performed using the IRAF/STSDAS task ELLIPSE. Setting the semi-major axis (sma) to  $0.2''$  (the size used for the light curve in Fig. 2 for this epoch) we find a position angle of  $17.4 \pm 0.1^\circ$  and an eccentricity of  $0.684 \pm 0.002$ . This can be compared with previous measurements with HST (P.A. =  $14 \pm 5^\circ$ )<sup>27</sup> and VLT/SINFONI (P.A. =  $15 \pm 0.9^\circ$ ,  $e = 0.83$ , from the  $1.644 \mu\text{m}$  Si I/Fe II feature)<sup>21</sup>. The agreement with the position angle is clearly good and, given that the SINFONI measurements probe the Si/Fe core and the R-band is dominated by the H-rich gas, the agreement with the eccentricity is also reasonable. As described in the main paper, the light curves presented in Fig. 2 were derived using this elliptical aperture. The size of the aperture was expanded as a function of time in order to always follow the same ejecta material.

In order to make sure that the transition from a decaying to a rising flux seen in Fig. 2 is not connected to the use of this particular aperture, we also performed the measurements using apertures with other shapes and sizes, trying both apertures that have a fixed size and apertures that expand with the ejecta. Supplementary Fig. 2 shows the R- and B-band light curves for the same expanding elliptical aperture as in Fig. 2, an expanding circular aperture (with radius equal to the sma of the elliptical aperture) as well as a large, fixed aperture. The fixed aperture encloses most of the ejecta but still avoids direct contamination by the ring (the aperture is shown in Fig. 1). The light curves extracted from the expanding elliptical and circular apertures show very similar

behaviour, demonstrating that the exact shape of the aperture is not important. The light curve from the large, fixed aperture also shows the same behaviour during the first  $\sim 7,000$  days, but levels off at late times. This is at least partly due to ejecta material expanding out of the fixed aperture. The large aperture is also likely to be significantly affected by contamination from the circumstellar ring, making it hard to draw firm conclusions regarding the ejecta using this aperture.

Contamination from the ring (due to flux from the brightening ring spilling into the ejecta region) is likely to affect all our light curves at some level. In order to quantify this effect we used the HST point-spread-function modelling tool Tiny Tim<sup>28</sup> and created models for the ring for a number of different epochs in both bands. We set up the models to match the observed distribution of hot spots as closely as possible and to have the same total flux in the ring area as the observations. The modelling is illustrated in Supplementary Fig. 3, which shows the real data and the model for the F675W image from 2009-04-29, and in Supplementary Fig. 4, which compares the radial profiles of the data and the model. The corrected light curves derived using these models are shown as open symbols in Fig. 2 and Supplementary Fig. 2. The contribution from the ring increases with time and is larger in the R-band, but it does not have a major effect on the light curves from the expanding apertures. For the large, fixed aperture the contamination is much more severe, reaching about 50% of the total flux at late times in the R-band.

The modelling of the ring is naturally associated with some uncertainties. In order to quantify these uncertainties we performed two different tests. First, we investigated the effect of varying the number of point sources used to model the ring. Specifically, we created models using between

8 and 90 point sources distributed along the ring, while always keeping the total flux in the ring area constant. The different ring models resulted in fluxes in the ejecta apertures that agreed to within 15%. This demonstrates that the specific model for the ring is not very important as long as the same total flux is distributed in an ellipse around the ejecta. The main reason for this is of course that we are interested in the total flux that leaks into the ejecta region and not its detailed distribution.

Another test of the models is to compare the flux in the synthetic and real images in regions located just outside the circumstellar ring. We used clean regions (uncontaminated by stars and other sources of emission) that allow us to measure the flux in the wings of the point sources in the ring. For the observation from 2009-04-29 we find that the agreement is excellent (the discrepancy is less than 10%), which gives us confidence that the models provide a good estimate of the emission from the ring. For earlier epochs it is harder to evaluate the models in this way since the clean regions outside the ring are completely dominated by the sky background rather than ring emission. For this reason we cannot determine whether our models are equally accurate at early times. We note, however, that the flux from the ring is negligible at these times.

An additional source of uncertainty is the loss of Charge Transfer Efficiency (CTE). This effect is known to increase with time and is especially important for faint objects on low backgrounds located far from the detector readout<sup>29</sup>. To investigate the importance of CTE losses we performed aperture photometry on about 10 stars of varying brightness located around SN 1987A. We found that the effect is negligible in the ACS but clearly noticeable in WFPC2, where stars lose

at most  $\sim 10\%$  of their flux between 1994 and 2009. This also agrees with estimates obtained for the supernova ejecta using the WFPC2 CTE correction formula<sup>29</sup>. In terms of the light curve in Fig. 2, we note that a  $\sim 10\%$  increase in the WFPC2 data points at late times would improve the agreement between the ACS and WFPC2.

## 2 Spectroscopy

As a complement to the photometry we investigate HST STIS spectra taken with the G750L grating in 2004 and 2010. These spectra overlap with the wavelength region covered by the R-filters and give us an opportunity to study the different spectral components that may contribute to the increase in flux. In both observations a slit with a width of  $0.2''$  was placed in the north-south direction, centred on the ejecta<sup>16,30</sup>. In 2004 there were also two observations taken with the narrow slit placed on either side of the central slit. To allow for a comparison with the photometry we extracted spectra in regions that match the size of the expanding elliptical aperture as closely as possible. This means using the central slit only and an extraction height of  $\pm 0.24''$  in 2004 and  $\pm 0.31''$  in 2010.

Supplementary Fig. 5 shows the  $H\alpha$  profiles from 2004 and 2010. The line profiles are clearly asymmetric with a strong blue wing extending down to  $\sim -5,000 \text{ km s}^{-1}$  and a red wing that only reaches velocities of about  $\sim 2,500 \text{ km s}^{-1}$ . The constant width of the ejecta line profile shows that the expanding aperture that we used follows the same material over a 6-year span of

time. From the two-dimensional spectra<sup>16,30</sup> it is clear that the blue wing mainly comes from the northern part of the ejecta. The lack of a correspondingly strong red wing may be due to dust absorption in the far side of the ejecta. Supplementary Fig. 5 also shows that the increase in flux between 2004 and 2010 is mainly due to an increase in the blue wing of the ejecta profile.

The  $H\alpha$  emission also contains a small contribution from the reverse shock. This component is clearly visible on the red side of the line as the boxy part of the profile between  $\sim 3,000 - 9,000 \text{ km s}^{-1}$ . On the blue side of the line the reverse shock appears at velocities higher than  $\sim -9,000 \text{ km s}^{-1}$ , where it is blended with the broad [O I]  $\lambda\lambda 6300, 6364$  lines from the ejecta at  $-12,022 \text{ km s}^{-1}$  and  $-9,096 \text{ km s}^{-1}$ . To estimate the flux from the reverse shock we focus on the boxy part of the profile on the red side, since this is not blended with any other strong lines. The contribution from this component compared to the total flux in the R-band is  $\sim 9 - 10\%$  in both 2004 and 2010. It is clear from inspection of the spectra that the reverse shock is not as strong on the blue side, and a very conservative upper limit on the total contribution from the reverse shock is therefore  $\sim 20\%$ . We especially note that there is no significant increase between 2004 and 2010.

In Supplementary Fig. 5 we also show the spectrum obtained by combining the three slit positions from the 2004 observations, renormalized to the continuum of the other spectra. The combined spectrum is very similar to that from the central slit, albeit with a slightly stronger line core and red wing. The contribution from the reverse shock on the red side is  $\sim 11\%$ , i.e. only marginally larger than the values given above.

The STIS observation from 2010 also allows us to investigate the emission from the south-

ernmost part of the ejecta, which is seen outside both the expanding and the fixed aperture at late times (Fig. 1). STIS spectra extracted in this region show a significant contribution from the reverse shock but also an asymmetric line profile from the ejecta, with a strong blue wing extending down to  $\sim -2,000 \text{ km s}^{-1}$ . The fact that we see blueshifted emission from the southern part of the ejecta shows that there must be some ejecta material located well above the plane of the ring.

The [Ca II] observations in Fig. 2 were performed between 2000 and 2009 with the Very Large Telescope (VLT) at ESO, using the UVES instrument. The primary purpose of these observations was to follow the evolution of the narrow lines from the ring collision. To maximise the spectral resolution and to minimise contamination from nearby stars a comparatively narrow slit,  $0.8''$  wide, was chosen. The seeing was in most cases  $0.6 - 0.8''$ , which is just enough to spatially resolve the ring into a northern and a southern part. The slit was centred on the position of the supernova and had a position angle of  $30^\circ$  in all the observations. The observations were reduced with the standard pipeline and the errors on the absolute fluxes were estimated to be less than 20 – 30% (ref. 5).

### **3 Modelling of the light curve**

At first, the energy radiated by a SN comes from the shock wave arriving at the surface of the exploding star. This phase lasted only a few hours in SN 1987A, and was followed by a period of a few weeks where the light curve was powered by the diffusive release of the internal



energy produced by the shock wave<sup>17</sup>. Subsequently, the energy for emission was supplied by the decay of radioactive isotopes created in the explosion. During the first  $\sim 1,000$  days the radioactive input was dominated by  $^{56}\text{Ni}$ , decaying into  $^{56}\text{Co}$  and  $^{56}\text{Fe}$ . From the first two years of the bolometric light curve the mass of  $^{56}\text{Ni}$  could be determined to  $0.069 M_{\odot}$ <sup>31</sup>. After  $\sim 1,000$  days  $^{57}\text{Ni}$  took over and a mass of  $3 \times 10^{-3} M_{\odot}$  was found<sup>32–34</sup>. Finally, after  $\sim 1,600$  days the next most abundant isotope,  $^{44}\text{Ti}$ , has been predicted to dominate the energy input to the ejecta. While the bolometric light curve could be accurately determined up to  $\sim 1,000$  days, the dominance of the mid-IR, which is difficult to determine from observations, requires accurate modelling of the optical bands at later times. In addition, the hydrogen-rich parts of the ejecta are subject to a freeze-out<sup>34</sup>, where recombination and cooling become slow compared to the radioactive decay time-scales and the expansion time-scales. It is therefore necessary to use a time-dependent approach for the modelling.

The modelling of the radioactively powered part of the light curves in Fig. 3 is based on a time-dependent spectral code<sup>35,36</sup>. The code includes calculations of the non-thermal excitation and ionization by the gamma-rays and positrons from the radioactive decay of  $^{56}\text{Ni}$ ,  $^{57}\text{Ni}$  and  $^{44}\text{Ti}$ , as well as a full non-local thermodynamic equilibrium treatment of the most important elements and lines. The present version also includes updated atomic data, in particular more accurate collision rates for Fe II, and other ions. The radiative transfer uses the Sobolev approximation, which treats the line escape in individual lines accurately. However, the non-local scattering from line to line is not included (except for the Ca II H and K lines, which feed the [Ca II]  $\lambda\lambda 7291.5, 7323.9$  lines by fluorescence). This especially affects the UV and blue parts of the spectrum and

leads to an underestimate of the flux in the B-band<sup>12</sup>.

An important test is that this model accurately reproduces the  $H\alpha$  evolution up to day 3,600 (ref. 2). A comparison with the spectrum at 7.8 years<sup>22</sup> shows agreement to within 50% for the R-band, but the model underestimates the flux in the B-band by a factor of 2.5. To model the shape of the light curves we therefore renormalize the B-band fluxes by a factor 2.5 and the R-band by a factor 1.5. The total energy input from radioactivity can be estimated to  $\sim 1.2 \times 10^{36} \text{erg s}^{-1}$  at 20 years<sup>12</sup>. In addition to this there is a substantial contribution from delayed recombination (freeze-out). This comes primarily from the low-density hydrogen envelope and is seen mainly as Balmer emission. The decrease of this component is substantially faster than the  $^{44}\text{Ti}$  decay and is responsible for the fast decline seen before  $\sim 4,000$  days (Fig. 3).

When translating the broad-band fluxes to luminosities we assume a distance of 50 kpc and a reddening of  $E_{B-V} = 0.16 \text{ mag}$ <sup>37</sup>. For the comparison with the observations we use the light curve from the expanding elliptical aperture, multiplied by a constant factor for the R- and B-bands. The reason for using this, rather than the fixed aperture in Fig. 1, is that the latter shows a misleading flattening at epochs later than  $\sim 7,000$  days because of the expansion of part of the ejecta outside the aperture. The constant factors were determined as an average of the ratio of the flux in the fixed aperture to that of the expanding aperture for epochs earlier than 7,000 days. The constants are 2.6 for the R-band and 2.5 for the B-band. There is of course some uncertainty in the correction from the expanding aperture to the total emitted flux, which also affects the  $^{44}\text{Ti}$  mass.

To determine the X-ray input to the ejecta we calculated the photoelectric absorption along

different rays in the ejecta from a point source located at the radius of the circumstellar ring. For the abundance and density distributions we used the partially mixed 14E1 explosion model<sup>17</sup>. This model is spherically symmetric (although mixed). Unfortunately, no 2-D or 3-D simulations exist with appropriate nucleosynthesis. The spherical approximation should, however, be sufficient for the qualitative nature of the model. Most of the envelope is transparent to X-rays with energies above about 0.2 keV as seen in Supplementary Fig. 6, which shows the ejecta expansion velocity for optical depth  $\tau = 1$  as a function of photon energy. The high metallicity core dominates the opacity by K- and L-shell absorption by oxygen and other elements, and is opaque at all but the very highest energies.

The energy deposition is an angular average of the absorbed intensity over all directions of the core and envelope, shown in Supplementary Fig. 7 for four different photon energies. The different deposition curves can be well approximated by  $C(E) \times 10^{-3} t_{\text{yr}}^{1.67}$ , where  $C(E) = (4.5, 1.6, 0.7) \times 10^{-3}$  for  $E = 0.1, 0.35,$  and  $1$  keV, respectively. The general time dependence can be explained as a balance between the increase of the solid angle of the core as seen from the ring,  $\propto t^2$ , and the increasing transparency of the ejecta as the density decreases.

The X-ray luminosity used in this paper is that directly observed by Chandra<sup>6</sup>. This is likely to be an underestimate for several reasons. The quoted X-ray luminosities only refer to the observed flux  $\gtrsim 0.5$  keV. For a shock with a temperature of 0.35 keV most of the luminosity is below this energy, especially if the shock is radiative, as is likely for shocks with velocities below  $\sim 400$  km s<sup>-1</sup> (ref. 3). In addition, the line profiles of the optical emission show that there

are shocks of lower velocities, most likely tangential shocks<sup>38</sup>, which radiate mainly below the observable X-ray band and add to the ionizing flux. The typical shock velocity from the optical lines is  $\sim 200 \text{ km s}^{-1}$  (ref. 5), which corresponds to a temperature of  $\sim 50 \text{ eV}$ . Because the opacity increases as  $E^{-3}$  (Where  $E$  is the photon energy), the absorption efficiency of the ejecta of this low energy radiation is nearly 100%. The absorbed X-rays are therefore more than enough to explain the observed increase in the optical bands. A more accurate estimate of the spectral distribution would require a detailed numerical calculation of the X-ray absorption and thermalization, which is beyond the scope of this paper. We also remark that both the optical emission from the ring<sup>5</sup> and the mid-IR<sup>8</sup> are strongly correlated with the X-rays.

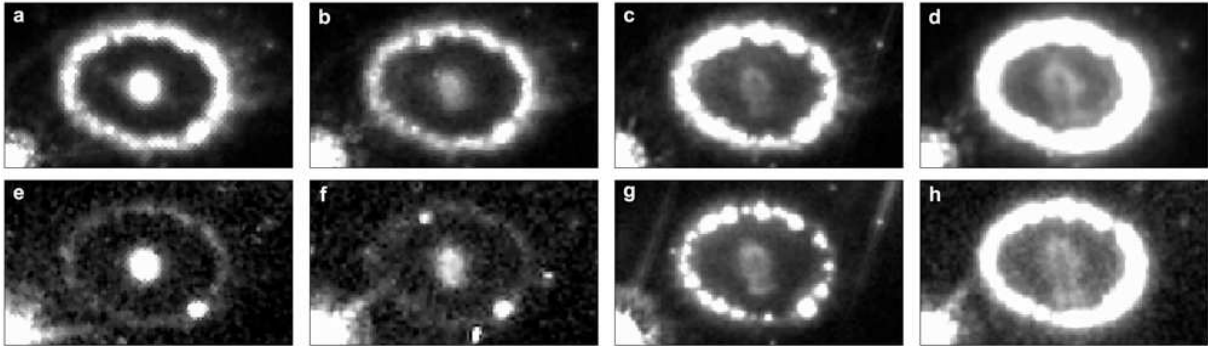
The conversion from X-rays to optical emission takes place first by photoelectric absorption, creating fast non-thermal electrons with energies up to keV. These are thermalized by excitation, ionization and heating of the free, thermal electrons. For hydrogen at the relevant degree of ionization, 35 – 40% of the secondary electron energy goes into ionization, followed by recombination, while  $\sim 8\%$  goes into direct excitation of  $n > 2$  (refs 39, 40). At 100 – 200 K,  $\sim 9\%$  of the ionization energy and  $\sim 16\%$  of the excitation energy emerges as  $H\alpha$  (ref. 41). In total this corresponds to  $\sim 5\%$  of the X-ray energy. Other elements add to this. The relative importance of excitation, ionization and heating will remain roughly constant as long as the ionization is  $\lesssim 10^{-2}$ , and we therefore do not expect conversion efficiency for the two bands to change over time. However, once the ionization surpasses this value, the fraction going into heating increases at the expense of the other channels. This will increase the far-IR fine structure lines compared to the optical lines until the temperature is high enough for thermal effects to increase the optical/UV emission<sup>35,36</sup>.

## 4 Effects of dust and positron leakage in the ejecta

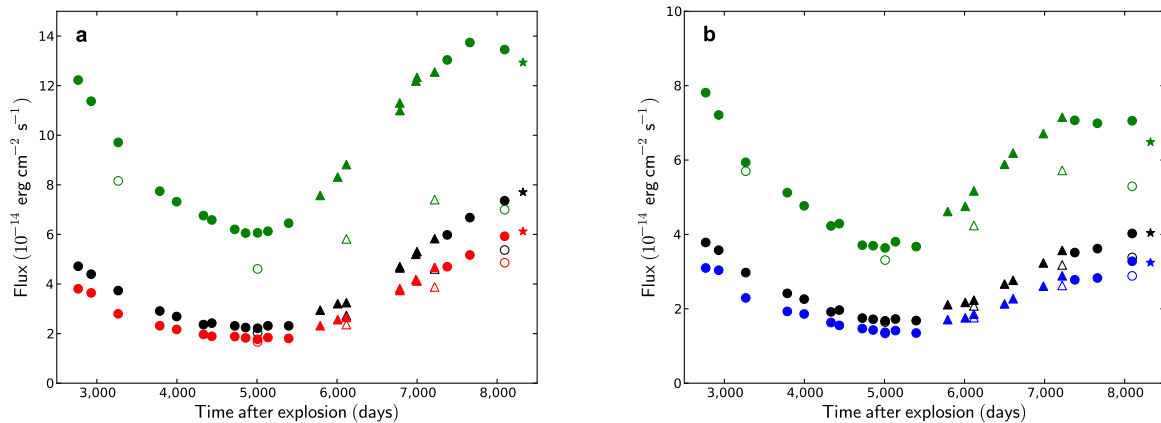
There is strong evidence for dust in the ejecta from early observations<sup>23,24,42</sup>, as well as from observations discussed in this supplement. In principle, a transition from optically thick to optically thin dust could account for an increase in the flux. This is, however, unlikely for several reasons. First, it would be a strange coincidence that this would occur at the same time as the X-ray flux becomes important. Secondly, compared to the flux from our model with constant covering fraction (i.e. optically thick dust clumps), which is given by the dashed line in Fig. 3, the increase has to be a factor of  $\sim 8$  in the R-band and  $\sim 5$  in the B-band. The estimated covering factor of the dust at early times was  $\sim 0.5$  (refs 23, 24), implying a maximum increase in the flux by a factor of  $\sim 2$ . Moreover, we expect the increase to occur first in the R-band and later in the B-band, based on the higher extinction in the latter band. The imaging also indicates dust obscuration in the central part of the SN up to the latest epochs (Supplementary Fig. 1), although this may also be an artefact of the external X-ray illumination, as discussed in the main paper.

Finally, positron leakage from the Fe-rich material containing the  $^{44}\text{Ti}$  may enhance the emission from the O- and H-rich zones in the core<sup>12</sup>. This depends sensitively on the strength of a magnetic field in the ejecta, which is uncertain. The main effect of positron leakage is that the hydrogen and intermediate element lines would increase at the expense of the Fe I-II lines. At most this may enhance the emission in the observed bands by a factor of  $\sim 2$  compared to the complete trapping case. As discussed above, this is far from sufficient to explain the observed increase in the R- and B-bands.

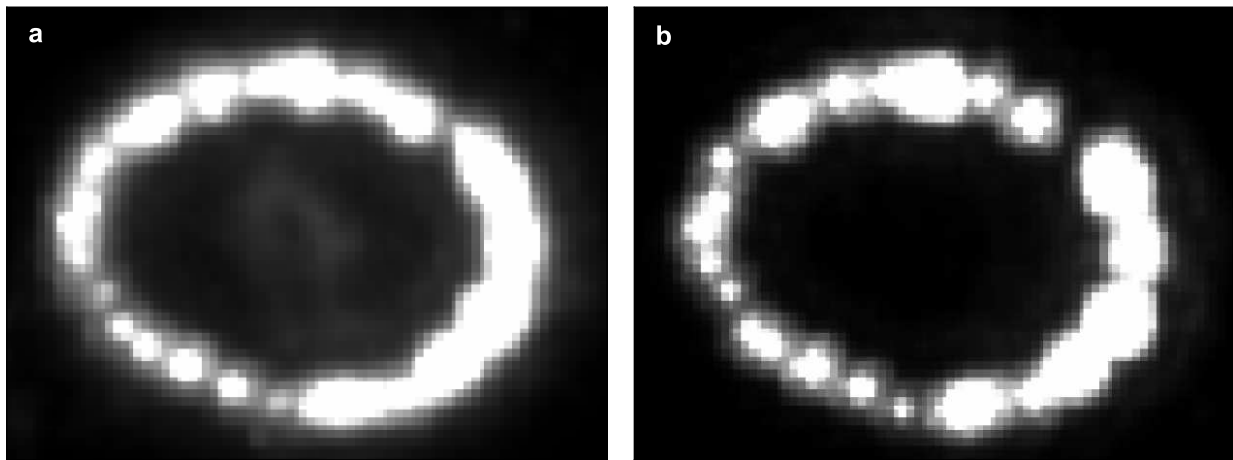
## 5 Supplementary Figures



Supplementary Figure 1: Selection of HST images of SN 1987A. The images show the evolution of the ejecta and the circumstellar ring as a function of time. The top row shows the R-band and the bottom row shows the B-band. The observing dates are 1994-09-24 (**a** and **e**), 1999-04-21 (**b** and **f**), 2003-11-28 (**c** and **g**) and 2009-04-09 (**d** and **h**), which correspond to 2,770, 4,440, 6,122 and 8,101 days after the explosion, respectively. Note the expansion of the ejecta and the brightening hot spots in the circumstellar ring.

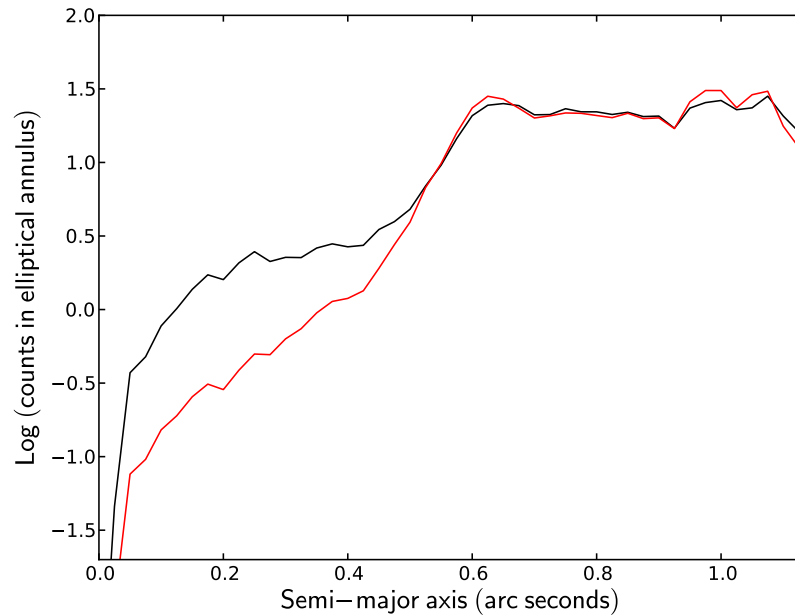


Supplementary Figure 2: Comparison of ejecta light curves for different apertures. Panel **a** shows the R-band and panel **b** shows the B-band (note the different scales on the y-axes). Data points from WFC2, ACS and WFC3 are shown as dots, triangles and stars, respectively. A correction factor has been applied to the ACS and WFC3 fluxes in order to account for the differences between these instruments and WFC2. The red and blue data points correspond to the same expanding elliptical aperture as in Fig. 2, shown here for reference. Green data points are for a fixed aperture that encloses as much of the ejecta as possible ( $sma = 0.50''$ , see also Fig. 1) while black data points are for an expanding circular aperture with radius equal to the semi-major axis of the expanding elliptical aperture. Open symbols indicate approximate flux levels after accounting for emission from the circumstellar ring. The light curve from the fixed aperture clearly levels off at late times. This is at least partly due to ejecta material expanding out of the aperture, but other effects may also contribute.

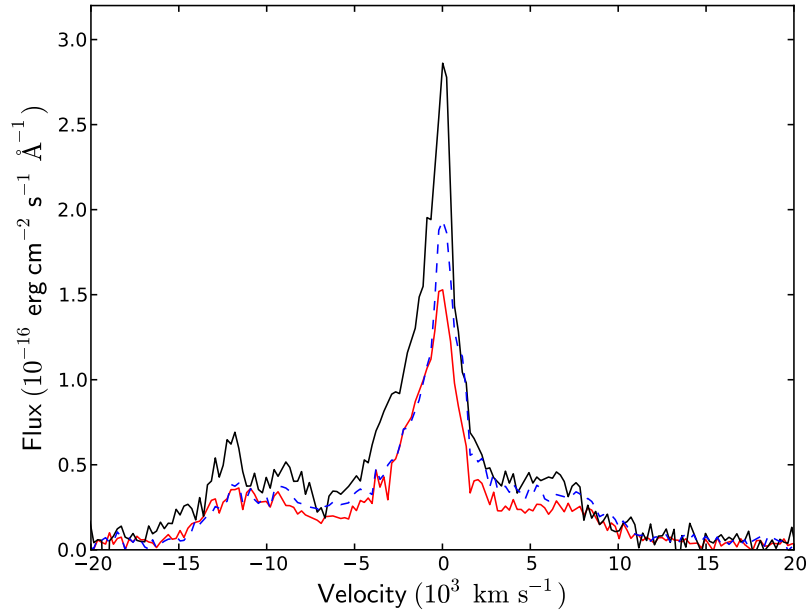


Supplementary Figure 3: Example of the modelling of the ring. **a**, The HST/WFPC2 F675W image from 2009-04-29. This is the same image as in Supplementary Fig. 1d but the image levels have been adjusted to show the structure of the ring more clearly. As a result the ejecta appear very faint. **b**, The model for the hot spots in the ring for the same epoch.

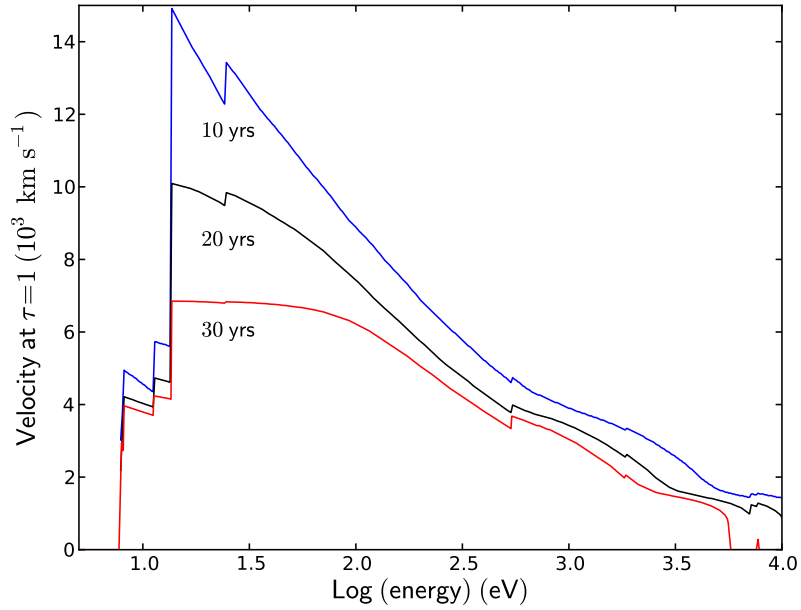




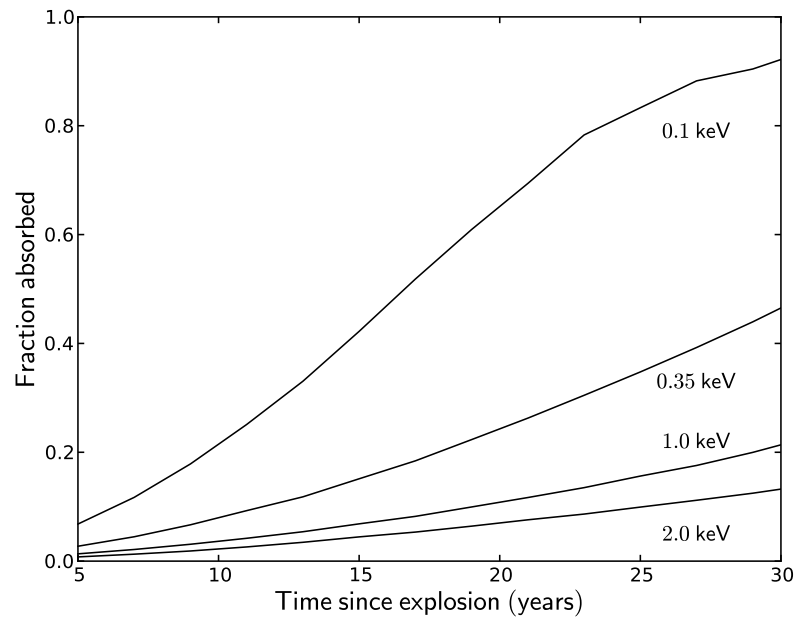
Supplementary Figure 4: Comparison of the radial brightness profiles of the real data and the model. The profiles were produced for the 2009-04-29 WFPC2/F675W observation (Supplementary Fig. 3), with the real data shown in black and the model in red. Specifically the lines show the counts inside elliptical annuli aligned with the circumstellar ring as a function of the sma of the annulus. The model clearly agrees well with the real data in the ring area (between about 0.6–1.0'') and should therefore give us a good estimate of the amount of flux from the ring that leaks into the ejecta region.



Supplementary Figure 5: STIS H $\alpha$  profiles of the ejecta. The red and black lines are for a 0.2'' slit placed in the north-south direction and centred on the ejecta in 2004 and 2010, respectively. The dashed blue line is the combined spectrum from three 0.2'' slits placed next to each other in 2004, renormalized to match the continuum level of the other spectra. The spectral extraction regions were chosen to correspond as closely as possible to the size of the expanding elliptical aperture used for the flux measurements in Fig. 2. The boxy part of the line profile between 3,000 and 9,000 km s $^{-1}$  is due to the reverse shock. There is also a contribution from the reverse shock on the blue side, but this is harder to disentangle, because of blending with the [O I]  $\lambda\lambda$  6300, 6364 lines at  $-12,022$  km s $^{-1}$  and  $-9,096$  km s $^{-1}$ .



Supplementary Figure 6: Ejecta velocity corresponding to optical depth  $\tau = 1$ . The optical depth is measured from the ring as a function of energy at 10, 20 and 30 years after the explosion. The maximum velocity for each of these curves is given by the ejecta velocity in the plane of the ring, which is  $2.1 \times 10^4 (t/10 \text{ yrs})^{-1} \text{ km s}^{-1}$ . Note the relatively small change in velocity with time of  $\tau(E) = 1$  for energies  $\gtrsim 0.2 \text{ keV}$ . The FWHM of the line profiles are therefore expected to decrease relatively slowly with time, as long as most of the shock energy is emitted above this energy. Note also that at 30 years the full ejecta will be transparent at  $\gtrsim 6 \text{ keV}$ .



Supplementary Figure 7: Fraction of the X-ray flux absorbed by the supernova ejecta as a function of time. The different lines correspond to different photon energies as indicated in the figure. The main reason for the evolution is the increasing solid angle of the core as seen from the ring ( $\propto t^2$ ), damped by the increasing transparency at higher energy.

## 6 Supplementary Table

Date	Instrument / Filter	Exposure time (s)	Instrument / Filter	Exposure time (s)
1994-09-24	WFPC2 / F675W	600	WFPC2 / F439W	800
1995-03-05	WFPC2 / F675W	600	WFPC2 / F439W	800
1996-02-06	WFPC2 / F675W	600	WFPC2 / F439W	950
1997-07-10	WFPC2 / F675W	600	WFPC2 / F439W	800
1998-02-06	WFPC2 / F675W	400	WFPC2 / F439W	500
1999-01-07	WFPC2 / F675W	1220	WFPC2 / F439W	1039
1999-04-21	WFPC2 / F675W	400	WFPC2 / F439W	800
2000-02-02	WFPC2 / F675W	400	WFPC2 / F439W	460
2000-06-16	WFPC2 / F675W	400	WFPC2 / F439W	800
2000-11-13	WFPC2 / F675W	2400	WFPC2 / F439W	1200
2001-03-23	WFPC2 / F675W	500	WFPC2 / F439W	1000
2001-12-07	WFPC2 / F675W	800	WFPC2 / F439W	1600
2003-01-05	ACS / F625W	800	ACS / F435W	1200
2003-08-12	ACS / F625W	480	ACS / F435W	800
2003-11-28	ACS / F625W	800	ACS / F435W	1600
2004-12-15			ACS / F435W	1600
2005-04-02			ACS / F435W	1200
2005-09-26	ACS / F625W	12000		
2005-09-28	ACS / F625W	720		
2006-04-15	ACS / F625W	1200	ACS / F435W	1200
2006-04-29	ACS / F625W	720		
2006-12-06	ACS / F625W	1200	ACS / F435W	1800
2007-05-12	WFPC2 / F675W	2700	WFPC2 / F439W	3000
2008-02-19	WFPC2 / F675W	1600	WFPC2 / F439W	2400
2009-04-29	WFPC2 / F675W	1600	WFPC2 / F439W	2000
2009-12-12	WFC3 / F625W	3000	WFC3 / F438W	800

Supplementary Table 1: HST observations used for the analysis.

## References

- [25] Wang, L. *et al.* Hubble Space Telescope Spectroscopic Observations of the Ejecta of SN 1987A at 2000 Days. *Astrophys. J.* **466**, 998–1010 (1996).
- [26] Tziamtzis, A., Lundqvist, P., Gröningsson, P. & Nasoudi-Shoar, S. The outer rings of SN 1987A. *Astron. Astrophys.* **527**, A35–A48 (2011).
- [27] Wang, L. *et al.* The Axisymmetric Ejecta of Supernova 1987A. *Astrophys. J.* **579**, 671–677 (2002).
- [28] Tiny Tim HST PSF Modeling, <http://www.stsci.edu/hst/observatory/focus/TinyTim>, (2011).
- [29] Dolphin, A. E. A Revised Characterization of the WFPC2 CTE Loss. *PASP* **121**, 655–667 (2009).
- [30] Heng, K. & McCray, R. Balmer-dominated Shocks Revisited. *Astrophys. J.* **654**, 923–937 (2007).
- [31] Bouchet, P. *et al.* The Bolometric Lightcurve of Supernova 1987A - Part Two - Results from Visible and Infrared Spectrophotometry. *Astron. Astrophys.* **245**, 490–498 (1991).
- [32] Kurfess, J. D. *et al.* Oriented Scintillation Spectrometer Experiment observations of Co-57 in SN 1987A. *Astrophys. J.* **399**, L137–L140 (1992).
- [33] Varani, G. F., Meikle, W. P. S., Spyromilio, J. & Allen, D. A. Direct Observation of Radioactive Cobalt Decay in Supernova 1987A. *Mon. Not. R. Astron. Soc.* **245**, 570–576 (1990).

- [34] Fransson, C. & Kozma, C. The freeze-out phase of SN 1987A - Implications for the light curve. *Astrophys. J.* **408**, L25–L28 (1993).
- [35] Kozma, C. & Fransson, C. Late Spectral Evolution of SN 1987A. I. Temperature and Ionization. *Astrophys. J.* **496**, 946–966 (1998).
- [36] Kozma, C. & Fransson, C. Late Spectral Evolution of SN 1987A. II. Line Emission. *Astrophys. J.* **497**, 431–457 (1998).
- [37] Fitzpatrick, E. L. & Walborn, N. R. Observations of Sk-69 deg 203 and the interstellar extinction towards SN 1987A. *Astron. J.* **99**, 1483–1487 (1990).
- [38] Pun, C. S. J. *et al.* Modeling the Hubble Space Telescope Ultraviolet and Optical Spectrum of Spot 1 on the Circumstellar Ring of SN 1987A. *Astrophys. J.* **572**, 906–931 (2002).
- [39] Xu, Y. & McCray, R. Energy degradation of fast electrons in hydrogen gas. *Astrophys. J.* **375**, 190–201 (1991).
- [40] Kozma, C. & Fransson, C. Gamma-ray deposition and nonthermal excitation in supernovae. *Astrophys. J.* **390**, 602–621 (1992).
- [41] Martin, P. G. Hydrogenic radiative recombination at low temperature and density. *Astrophys. J. Supp.* **66**, 125–138 (1988).
- [42] Moseley, S. H., Dwek, E., Glaccum, W., Graham, J. R. & Loewenstein, R. F. Far-infrared observations of thermal dust emission from supernova 1987A. *Nature* **340**, 697–699 (1989).